Structure, Electronic, and Vibrational properties of Salbutamol using Quantum Chemical and Molecular Docking Approaches

Dipak Joshi, Bhawani Datt Joshi*

Department of Physics, Siddhanath Science Campus, Tribhuvan University Mahendranagar, 10400

Research Article

ISSN: 3059-9504 (online)
DOI: https://doi.org/10.3126/ajs.v2i1.87744

Article History

Received: August 12, 2025; Revised: October 05, 2025; Accepted: October 10, 2025; Published: December 25, 2025

Keywords

Salbutamol, Density Functional Theory, β_2-Adrenergic Receptor, Molecular Docking, Vibrational Analysis, HOMO–LUMO, Drug Binding

***Corresponding author**

Email: bhawani.joshi@snsc.tu.edu.np (BD Joshi)
Orcid: https://orcid.org/0000-0003-3276-9319

ABSTRACT

Molecular structure, vibrational spectra, electronic properties, and receptor binding mechanism Salbutamol, a short-acting β_2-adrenergic agonist used in asthma therapy, were studied using density functional theory (DFT) and molecular docking methods. The molecular geometry was optimized at the DFT/B3LYP/3-21G level of theory. The calculated rotational constants are A = 0.917 GHz, B = 0.209 GHz, and C = 0.182 GHz provide insights into the molecular moments of inertia. The HOMO-LUMO energy gap was found to be 5.14 eV in the gas phase, decreasing in polar solvents, which indicated enhanced electronic polarization. Time-dependent DFT (TD-DFT) simulations revealed strong $\pi \rightarrow \pi^*$ electronic transitions in the near-ultraviolet region. Molecular docking of Salbutamol into the binding site of the human β_2-adrenergic receptor (PDB ID: 3NY8) yielded a binding affinity of -7.545 kcal/mol. The docking pose shows that Salbutamol forms hydrogen bonds with ASP113 and ASN312, and engages in hydrophobic contacts with VAL114, VAL117, and PHE290. These structural and electronic insights rationalize the known biological activity of Salbutamol and may guide the future design of improved β_2-agonist drugs.

1. INTRODUCTION

Salbutamol, also known as Albuterol and chemically as 4-[2-(tert-butylamino)-1-hydroxyethyl]-2-(hydroxymethyl)phenol, is a selective β_2-adrenergic receptor agonist widely used to manage acute bronchospasm in asthma and chronic broncho-pulmonary conditions [1]. Its white crystalline powder structure includes a benzene ring inclined at 74.5° and a *tert*-butyl group positioned opposite amino and hydroxy groups, contributing to its high receptor selectivity and potent smooth muscle relaxation in the lungs [2,3]. It is administered primarily by inhalation for rapid onset within 5 minutes, with effects lasting up to 14 hours if taken orally [4,5]. Besides bronchodilation, Salbutamol influences cardiovascular, uterine, metabolic, and neurological systems [6,7,8]. High systemic doses may cause side effects such as tachycardia, but therapeutic inhalation doses have minimal impact on physical performance, leading to its regulation by WADA since 2004 [9]. The molecular structure of title molecule is shown in Fig. 1.

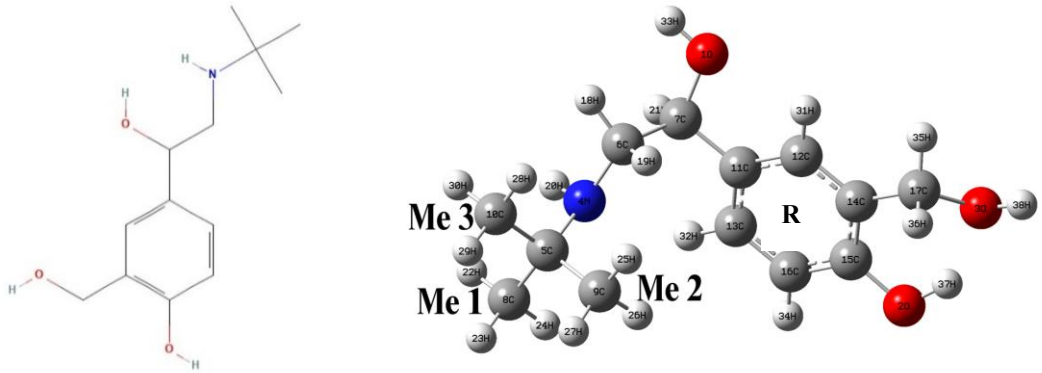

Fig. 1: (a) Molecular Structure of Salbutamol (source: PubChem) (b) Optimized structure of Salbutamol molecule using symbol and labelling of atom.

Apart from asthma and COPD, Salbutamol is also prescribed to prevent exercise-induced bronchospasm and explored for its potential benefit in acute respiratory distress syndrome by enhancing alveolar fluid clearance and reducing inflammation.

Literature reveals that Ali et al. (2009) studied Salbutamol hemisulphate using FT-Raman, IR, and DFT to identify vibrational modes linked to hydrogen bonding [10]. Zhao et al. (2020) analyzed Salbutamol binding to human serum albumin using spectroscopy and docking, revealing binding-induced conformational changes [14While previous studies have focused on specific aspects of Salbutamol, such as its crystallographic disorder or binding to serum albumin, a comprehensive theoretical study integrating its detailed structural, vibrational, and electronic properties with its binding mechanism to the β_2-adrenergic receptor is lacking. Therefore, this study aims to bridge this gap by providing a unified computational characterization of Salbutamol using DFT and molecular docking to bridge this gap and establish a solid structure activity relation.

2. MATERIALS AND METHODS

In this work, the initial molecular geometry of Salbutamol was retrieved from the PubChem database [15]. Geometry optimization was performed using Density Functional Theory (DFT) at the B3LYP/3-21G level of theory without any geometric constraints, employing the Gaussian 09 software package [16].
Following optimization, vibrational frequency calculations were conducted at the same level of theory to confirm the optimized structure corresponds to a minimum on the potential energy surface (no imaginary frequencies), yielding 108 vibrational modes as predicted by the formula 3N-6, where N is the number of atoms [17]. Potential energy distribution (PED) was analyzed using GAR2PED software, which utilizes internal coordinates and localized symmetry following Pulay's recommendations [18,19]. Visualization of the calculated IR and Raman vibrational spectra was conducted using GaussView, and the intensities were plotted using OriginPro 7 software [20]. To correct the systematic overestimation of vibrational wavenumbers common in DFT methods, scaling was applied using the wavenumber linear (WLS) approach as follows: $\ddot{\upsilon}_{obs} = (1.0087 - 0.0000163 \times \ddot{\upsilon}_{cal}) \times \ddot{\upsilon}_{cal}$ [21]. Electronic excitation spectra were predicted with time-dependent DFT (TD-DFT) calculations to evaluate excited states, electronic transitions, and oscillator strengths [22].

Molecular docking studies were carried out using SwissDock, which applies EADock DSS algorithms, with AutoDock Vina parameters for ligand and receptor preparation [23,24,25]. The three-dimensional structure of the target protein, the human β_2-adrenergic receptor (PDB ID: 3NY8), was selected as it is a high-resolution structure co-crystallized with a bound ligand, providing a reliable model for studying agonist binding. This structure was obtained from the RCSB Protein Data Bank and used without modification for docking studies. Salbutamol's ligand structure was provided in SMILES format and automatically converted to a 3D energy-minimized form prior to docking.

All computational and docking visualizations were systematically processed using GaussView, GAR2PED, Discovery Studio, and OriginPro 7 to support detailed structural and interaction analyses.

3. RESULTS AND DISCUSSION

3.1 Geometry Optimization

The optimized molecular geometry of Salbutamol consists of a substituted phenylethanolamine backbone, including a benzene ring, an aliphatic side chain, and polar functional groups such as hydroxyl and secondary amine. The geometry was optimized using the DFT/B3LYP/3-21G level of theory, and the structural parameters such as bond lengths, bond angles, and dihedral angles are summarized in Table 1.

Table 1: Optimized geometric parameters of Salbutamol at B3LYP/3-21G level

Bond Length		Bond Angle		Dihedral Angle	
Optimized Parameters	Value (Å)	Optimized Parameters	Value (º)	Optimized Parameters	Value (º)
O1-C7	1.466	C7-O1-H33	107.4	H33-O1-C7-C6	-66.6
O1-H33	0.993	C5-C4-C6	117.9	H33-O1-C7-C11	171.3
O2-C15	1.375	C5-C4-H20	109.3	C6-N4-C5-C8	175.8
O2-H37	1.018	C6-N4-H20	109.9	C6-N4-C5-C9	-66.8
O3-C17	1.490	N4-C5-C9	109.1	C5-N4-C6-C7	167.9
O3-H38	0.993	C7-C6-H18	107.6	C9-C5-C8-H22	179.4

N4-C5	1.499	O1-C7-C6	108.2	C9-C5-C8-H23	59.6
N4-C6	1.477	C6-C7-C11	113.2	C9-C5-C8-H24	-60.9
N4-H20	1.028	C5-C8-H23	110.4	O1-C7-C11-C12	-5.7
C5-C8	1.544	C5-C8-H24	109.5	O1-C7-C11-C13	175.6
C6-H18	1.107	H22-C8-H23	108.3	C6-C7-C11-C12	-124.7
C7-C11	1.520	C7-C11-C13	121.5	C6-C7-C11-C13	56.6
C7-H21	1.103	C12-C14-C15	120.0	C7-C11-C12-C14	-179.4
C11-C12	1.396	C15-C14-C17	119.9	C12-C14-C15-O2	178.4
C11-C13	1.403	O2-C15-C14	122.3	C12-C14-C15-C16	-1.4
C12-C14	1.396	O2-C15-C16	119.1	C17-C14-C15-O2	-6.0
C13-C16	1.390	C14-C15-C16	118.6	C17-C14-C15-C16	174.2
C13-H32	1.082	C13-C16-C15	121.1	C12-C14-C17-O3	-146.7
C14-C15	1.409	C13-C16-H34	121.3	C12-C14-C17-H35	-25.9
C14-C17	1.511	C15-C16-H34	117.7	C12-C14-C17-H36	93.8
C15-C16	1.401	O3-C17-C14	108.9	O2-C15-C16-C13	-179.4

The aromatic ring comprises carbon atoms C11 to C16. The bond lengths within this ring are nearly uniform, with values such as C11-C12 = 1.396 Å, C11-C13 = 1.403 Å, C12-C14 = 1.396 Å, and C13-C16 = 1.390 Å. These values are consistent with the expected range for delocalized C-C bonds in a benzene ring. The bond angles between the ring carbons, such as C11-C12-C14 = 121.2° and C12-C14-C15 = 120.0°, further support the sp^2 hybridization and planarity of the ring system. At the para position of the aromatic ring, a hydroxyl group is attached through the C15-O2 bond, with a length of 1.375 Å. The O1-C7 bond is 1.466 Å in length, consistent with a typical C-O single bond.

The secondary amine nitrogen N4 is bonded to C5 and C6 with lengths of 1.499 Å and 1.477 Å, respectively. The N-H bond (N4-H20) is calculated to be 1.028 Å. These values are in agreement with standard C-N and N-H bond lengths found in similar molecular frameworks. The three methyl groups: Me1(C8), Me2(C9), and Me3(C10) are attached to the central carbon C5. Each C-C bond between C5 and the methyl groups lies in the range of 1.542-1.550 Å, which is characteristic of single bonds between sp^3 hybridized carbons. Dihedral angles across the aromatic-substituted region also indicate slight deviations from complete planarity. For example, the dihedral angle O1-C7-C11-C12 is -5.6°, while C7-C11-C12-C14 is -179.4°, showing the ring system and side chain are almost coplanar. On the other end, the tail of the molecule containing C17 and O3 has a twisted arrangement, as observed in C14-C17-O3-H38 = -166.1°.

3.2 **Mulliken Atomic Charges**

Among all atoms, the oxygen atoms exhibit the most negative Mulliken charges, consistent with their strong electronegativity. Specifically, atom O2 has the most negative charge of -0.64282, followed by atom N4 (-0.56011) and atom O1 (-0.55171). The carbon atoms in Salbutamol display a wide range of charge distributions. Atom C15 stands out with the highest positive Mulliken charge of +0.291077, indicating a significantly electron-deficient site likely to undergo nucleophilic attack or serve as a binding interface for electron-rich partners. The hydrogen atoms in Salbutamol show predominantly positive Mulliken charges, as expected due to their bonding to more electronegative atoms. Notably, H37 and H38 possess the highest positive values of +0.363623 and +0.35796, respectively, indicating strong polarization and their potential to act as hydrogen bond donors in biological interactions. Mullikan atomic charges are listed in Table 2 and plotted in Fig. 2.

Table 2: Mulliken Atomic charge of Salbutamol

Atoms	Mulliken Atomic Charge	Atoms	Mulliken Atomic Charge	Atoms	Mulliken Atomic Charge
O1	-0.55171	C14	-0.02906	H27	0.179326
O2	-0.64282	C15	0.291077	H28	0.187725
O3	-0.54628	C16	-0.18482	H29	0.184907
N4	-0.56011	C17	-0.1999	H30	0.174804
C5	0.025053	H18	0.149599	H31	0.198251
C6	-0.21105	H19	0.228297	H32	0.202864
C7	-0.01237	H20	0.263248	H33	0.33596
C8	-0.5076	H21	0.182942	H34	0.188266
C9	-0.50684	H22	0.173372	H35	0.208931
C10	-0.52317	H23	0.184967	H36	0.205416
C11	-0.00883	H24	0.202907	H37	0.363623
C12	-0.19306	H25	0.185208	H38	0.35796
C13	-0.2063	H26	0.209205		

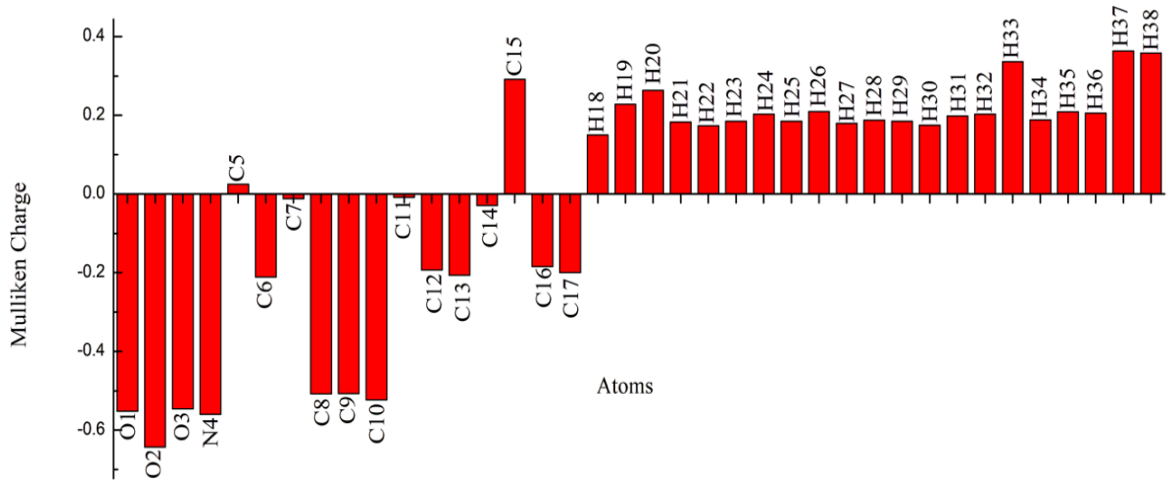

Fig. 2: Mulliken atomic charge vs atoms.

3.3 Vibrational Assignment

The vibrational spectra of Salbutamol were analyzed using Density Functional Theory (DFT) and Hartree-Fock (HF) calculations, providing insights into the nature of molecular bonding and intramolecular interactions. The calculated vibrational wavenumers are listed in Table 3. The IR and Raman spectra are given in Figs. 3 and 4, respectively.

Table 3: Vibrational wavenumbers (cm^{-1}), Raman Activity ($Å^4$/amu), IR intensity (km/mol), and their potential energy distribution.

Wavenumber			Raman Activity	IR Intensity	Potential Energy Distribution (PED) (≥ 5%)
Unscaled	Scaled				
DFT	DFT	HF			
3505	3336	3683	378.6	1.79	υ(O3H)(100)

3496	3327	3676	193.4	2.15	υ(O1H)(100)
3385	3227	3521	66.2	2.51	υ(NH)(100)
3237	3094	3489	142.4	7.78	R[υ(C13H)(80)+υ(C16H)(18)]
3231	3089	3257	42.7	1.40	R[υ(C12H)](98)
3219	3078	3246	69.3	5.12	R[υ(C16H)(81)+υ(C13H)(18)]
3142	3008	3233	67.6	21.87	Me2[$\upsilon(CH_3)$](48)+$\upsilon(C6H_2)$(40)+Me1[$\upsilon(CH_3)$](5)
3139	3005	3164	41.7	30.91	$\upsilon(C6H_2)$(50)+Me2[$\upsilon(CH_3)$](29)+Me1[$\upsilon(CH_3)$](19)
3133	3000	3143	25.8	8.32	Me1[$\upsilon(CH_3)$](70)+Me2[$\upsilon(CH_3)$](20)
3120	2988	3130	91.9	54.17	Me2[$\upsilon(CH_3)$](51)+Me3[$\upsilon(CH_3)$](38)
3113	2983	3117	10.8	4.09	Me3[$\upsilon(CH_3)$](58)+Me2[$\upsilon(CH_3)$](37)
3110	2979	3110	95.4	34.59	Me1[$\upsilon(CH_3)$](61)+Me3[$\upsilon(CH_3)$](29)
3103	2973	3108	11.2	4.33	Me3[$\upsilon(CH_3)$](65)+Me1[$\upsilon(CH_3)$](34)
3092	2963	3102	147.6	496.92	υ(O2H) (93)+$\upsilon(C17H_2)$(6)
3072	2945	3101	52.0	89.81	$\upsilon(C17H_2)$ (94) +υ(O2H)(6)
3059	2933	3069	145.6	6.87	Me2[$\upsilon(CH_3)$](94)
3046	2921	3055	120.9	31.35	Me1[$\upsilon(CH_3)$](56) +Me3[$\upsilon(CH_3)$](38)
3041	2916	3052	3.2	15.60	Me3[$\upsilon(CH_3)$](59)+Me1[$\upsilon(CH_3)$](40)
3003	2882	3049	125.4	58.30	$\upsilon(C17H_2)$(99)
2969	2851	3047	112.3	59.00	υ(C7H)(98)
2923	2809	2989	104.9	99.71	$\upsilon(C6H_2)$(98)
1669	1638	1764	9.8	44.41	R[υ(CC)(43)+δ(CHO)(23)+δ_a(5)+δ_{in}(CO)(5)+δ_{in}(C12H)(5)]
1633	1604	1724	42.9	52.10	R[υ(CC)(49)+δ(CHO)(16)+δ_{in}(C13H)(11)+δ_a(7)]
1583	1556	1660	1.7	13.93	Me2[(δ_a(34)+δ_a'(5)+ρ'(5))(CH_3)]+Me1[(δ_a(15)+δ_a'(14))(CH_3)]+Me3[(δ_a'(10)+δ_a(6))(CH_3)]
1573	1546	1656	12.7	5.87	Me3[$\delta_a(CH_3)$](43)+Me1[(δ_a(19)+δ_a'(14))(CH_3)+ρ(NH)(8)
1566	1540	1651	20.2	7.48	Me2[$\delta_a'(CH_3)$](49)+Me3[(δ_a'(23)+δ_a(6))(CH_3)]+Me1[$\delta_a'(CH_3)$](9)
1564	1538	1647	15.8	13.54	$\delta_{sc}(C17H_2)$(79)+$\delta_{sc}'(C17H_2)$(6)
1560	1533	1645	19.8	2.82	$\delta_{sc}(C6H_2)$(56)+Me1[$\delta_a(CH_3)$](18)+$\delta_{sc}(C17H_2)$(6)+Me1[$\delta_a'(CH_3)$](5)+Me2[δ_a(CH$_3$)](5)
1551	1525	1640	11.2	3.79	Me2[$\delta_a(CH_3)$](29)+$\delta_{sc}(C6H_2)$(28)+Me1[$\delta_a'(CH_3)$](18)+Me1[$\delta_a(CH_3)$](13)
1549	1523	1629	31.9	1.75	Me3[(δ_a'(32)+δ_a(21))(CH_3)+Me1[$\delta_a'(CH_3)$](22)+Me2[$\delta_a(CH_3)$](13)
1547	1521	1626	5.0	59.18	R[υ(CC)(41)+δ_{in}(C12H)(9)+δ_{in}(C17C)(9)+υ(CO2)(6)+δ(CHO)(5)]+ω($C17H_2$)(6)
1542	1517	1621	9.8	0.73	Me2[(δ_a'(35)+δ_a(5))(CH_3)]+Me3[(δ_a'(21)+δ_a(11))(CH_3)]+Me1[(δ_a(11)+δ_a'(6))(CH_3)]
1529	1504	1611	5.2	117.05	R[υ(CC)(24)+δ(CHO)(22)+δ_{in}(C16H)(19)+δ_{in}(C13H)(8)]+$\delta_{sc}(C17H_2)$(5)
1516	1492	1590	7.7	12.61	ρ(NH)(71)+Me1[$\delta_a(CH_3)$](7)
1468	1446	1560	1.7	14.25	Me2[$\delta_s(CH_3)$](38)+Me1[$\delta_s(CH_3)$](29)+Me3[$\delta_s(CH_3)$](24)
1447	1426	1537	6.3	31.85	R[υ(CC)(24)+δ_{in}(C13H)(18)+υ(CC)(11)+δ_{in}(C12H)(10)+δ(CHO)(6)+υ(CC17)(6)]
1444	1423	1536	4.8	25.91	Me2[$\delta_s(CH_3)$](52)+Me3[$\delta_s(CH_3)$](29)+Me1[$\delta_s(CH_3)$](10)

1443	1422	1533	2.3	18.09	Me1[$\delta_s(CH_3)$](50)+Me3[$\delta_s(CH_3)$](28)
1437	1416	1524	18.7	31.08	δ(CHO)(16)+ρ(CH)(15)+Me3[$\delta_s(CH_3)$](13)+(ω(10)+γ(6))($C6H_2$)+ρ'(CH)(10)+R[υ(C11C)](8)
1423	1402	1509	23.5	10.04	ω($C17H_2$) (60) +δ(CHO3) (15) +R[υ(CC17)](8)
1388	1369	1487	21.1	9.98	ω($C6H_2$)(53)+ρ'(CH)(22)+υ(CC)(5)
1354	1336	1443	16.7	0.31	ρ(CH)(36)+(ω(18)+γ(6))($C6H_2$)+ρ'(CH)(17)+δ(CHO)(7)
1345	1327	1407	12.1	22.81	R[υ(CC)](51)+δ_{in}(C16H)(9)+δ_{in}(C12H)(5)+δ_{in}(C17C)(5)]+ρ(CH)(6)
1315	1298	1396	6.3	1.13	R[υ(CC)(24)+δ_{in}(C12H)(16)+υ(CC17)(8)+δ_{in}(C13H)(5)]+ρ'(CH)(5)
1309	1293	1375	5.5	11.20	γ($C6H_2$)(16)+υ(C9C)(9)+υ(C5N)(7)+Me3[ρ'(CH_3)](6)+δ_{oop}(NC5C)(6)+Me1[ρ(CH_3)](5)+δ_{sc}(NH)(5)+R[δ_{in}(C12H)](5)
1298	1282	1363	3.1	112.87	R[υ(CO2(39)+δ_{trig}(13)+υ(CC)(13)+δ(CHO)(9)+δ_{in}(C13H)(6)]
1271	1256	1356	0.9	33.99	Me2[ρ(CH_3)](20)+υ(C8C)(19)+δ_{oop}(NC5C)(11)+Me3[ρ(CH_3)](10)+υ(C10C)(5)+ρ(NC5C)(5)
1263	1248	1350	4.5	46.31	δ(CHO3)(20)+R[υ(CC)(27)+δ_{trig}(7)+δ_{in}(C16H)(6)+υ(CC17)(5)]+ω($C17H_2$)(12)
1253	1238	1336	3.1	58.02	Me1[ρ'(CH_3)](17)+Me2[ρ'(CH_3)](16)+υ(C10C)(14)+δ_{oop}(NC5C)(15)+υ(C5N)(9)+γ($C6H_2$)(6)
1244	1230	1320	23.1	28.62	γ($C17H_2$)(57)+R[υ(CC)(7)+δ_{in}(C12H)(5)]+δ(CHO3)(6)
1240	1226	1303	6.4	8.88	ρ'(CH)(19)+γ($C17H_2$)(11)+γ($C6H_2$)(9)+ρ(CH)(7)+δ(CHO)(5)+R[υ(CC)](5)
1230	1216	1273	12.6	4.12	γ($C6H_2$)(26)+ρ(CH)(14)+δ(CHO)(10)+ρ(NH)(5)
1202	1188	1253	19.4	37.34	δ(CHO3)(18)+δ(CHO)(18)+R[δ_{in}(C16H)(8)+υ(CC)(8)+δ_{in}(C13H)(6)+υ(CC17)(6)]+ρ(CH)(8)
1178	1165	1240	5.8	23.32	R[υ(CC)(14)+δ_{in}(C16H)(14)+δ_{trig}(11)+υ(C11C)(10)+δ_{in}(C13H)(10)+δ_{in}(C12H)(7)]+δ(CHO)(7)
1139	1128	1205	4.6	58.92	R[υ(CC)(22)+δ_{trig}(12)+υ(CC17)(11)+δ_{in}(C12H)(11)+υ(C11C)(6)]+δ(CHO3)(7)+ρ($C17H_2$)(6)
1119	1108	1194	5.2	22.78	υ(C6N)(19)+Me2[ρ'(CH_3)](11)+ρ($C6H_2$)(9)+Me1[ρ'(CH_3)](9)+δ_{sc}(NH)(7)+Me3[ρ(CH_3)](7)+υ(CC)(5)+δ_{oop}(CH)(5)
1092	1082	1182	8.1	9.88	υ(C6N)(40)+υ(CC)(15)+ρ($C6H_2$)(11)+υ(C5N)(9)+δ_{oop}(CH)(5)
1074	1065	1151	8.3	3.01	Me3[(ρ'(34)+ρ(7))(CH_3)]+Me1[ρ(17)+ρ'(6))(CH_3)]+Me2[ρ(CH_3)](11)+υ(C6N)(5)
1058	1049	1150	6.2	31.53	Me2[ρ'(CH_3)](21)+Me1[ρ'(CH_3)](13)+υ(CC)(10)+υ(CO1)(9)+ρ($C6H_2$)(7)+υ(C6N)(6)+δ_{oop}(CH)(5)
1042	1033	1142	2.3	1.75	R[δ_{oop}(C13H)(23)+δ_{oop}(C16H)(11)+δ_{oop}(C12H)(5)+τ'$_a$(5)]+ρ($C17H_2$)(27)+υ(CO1)(5)
1039	1030	1132	1.4	5.82	R[δ_{oop}(C13H)(30)+δ_{oop}(C16H)(14)+Puck(14)]+ρ($C17H_2$)(9)+υ(CO1)(9)
1030	1022	1117	1.6	43.25	υ(CO1)(40)+ρ($C17H_2$)(16)+δ_{oop}(CH)(10)+δ_{sc}'($C6H_2$)(5)
1009	1001	1100	6.6	16.68	ρ($C6H_2$)(14)+υ(CC)(14)+υ(CO3)(9)+ρ($C17H_2$)(8)+R[υ(CC)](7)
998	991	1074	0.0	0.06	Me2[ρ(CH_3)](28)+Me1[ρ(CH_3)](25)+Me3[ρ(CH_3)](23)+Me1[ρ'(CH_3)](7)+Me3[ρ'(CH_3)](6)+Me2[ρ'(CH_3)](6)
983	976	1065	14.5	31.81	υ(CO3)(47)+R[δ_{oop}(C12H)](14)+υ(CC)(8)
955	949	1056	5.5	17.15	R[δ_{oop}(C12H)](43)+R[Puck](6)+υ(C9C)(6)
947	941	1005	8.9	9.18	R[δ_{oop}(C12H)](22)+υ(C9C)(17)+υ(C8C)(9)+ρ($C6H_2$)(7)+Me1[ρ(CH_3)](5)+Me3[ρ(CH_3)](5)
925	919	989	10.3	0.28	υ(C8C)(27)+υ(C10C)(20)+Me3[ρ'(CH_3)](10)+Me3[ρ(CH_3)](9)+Me2[ρ(CH_3)](8)+Me1[ρ'(CH_3)](5)
923	917	982	6.9	9.48	R[τ(CO)(11)+δ_{trig}(10)+δ_a(9)+υ(CC17)(9)+δ_{oop}(C12H)(8)]+υ(CO_3)(5)+υ(CC)(5)
912	906	977	5.9	2.97	υ(C5N)(25)+υ(C10C)(16)+Me2[ρ'(CH_3)](7)+Me1[ρ'(CH_3)](6)+υ(C8C)(6)+R[δ_{oop}(C16H)](6)

896	891	967	1.7	102.40	R[δ_{oop}(C16H)(36)+δ_{oop}(C13H)(17)+δ_{oop}(CO)(16)+τ_a(8)+Puck(6)]
889	884	877	5.2	95.97	R[τ(CO)](61)+υ(CO3)(12)
790	787	835	1.5	2.92	R[Puck(56)+δ_{oop}(CO)(18)+δ_{oop}(C17C)(9)+δ_{oop}(C11C)(6)]
784	781	795	11.9	17.80	R[υ(CC)(16)+υ(CO2)(15)+Puck(10)+δ_{trig}(6)+δ'_a(6)+υ(C11C)(6)+υ(CC17)(5)]
749	747	780	8.3	8.65	υ(C9C)(26)+υ(C10C)(22)+(δ(12)+δ_{sc}(9))(NH)+υ(C8C)(11)
743	741	776	7.4	11.24	R[δ'_a(12)+υ(C11C)(10)+δ_{trig}(7)+υ(CC)(6)+υ(CC17)(6)]+δ_{oop}(CH)(17)+δ_{sc}'($C17H_2$)(6)+δ(NH)(5)
700	699	725	5.9	91.68	δ(NH)(45)+υ(C5N)(12)+υ(C6N)(9)+δ_{sc}(NH)(7)+δ_{sc}'($C6H_2$)(5)
661	660	714	4.6	14.48	R[δ'_a(24)+δ_{oop}(C11C)(7)+τ_a(7)+δ_{in}(CO)(7)+δ_{oop}(C17C)(5)]+δ_{sc}'($C17H_2$)(18)
620	619	673	0.8	12.35	R[τ_a(19)+δ_{oop}(CO)(16)+δ_{oop}(C11C)(13)]+δ_{oop}(CH)(10)+δ_{sc}'($C17H_2$)(5)
562	562	611	2.1	18.23	δ_{oop}(CH)(28)+R[δ_a(14)+τ_a(7)+Puck(5)]
523	523	559	1.0	16.54	δ_{oop}(CH)(17)+ρ(NC5C)(16)+R[Puck(6)+τ_a(5)+δ_{oop}(CO)(5)]+δ_{sc}(NH)(14)
512	512	541	4.3	5.21	R[δ_{in}(CO)(10)+δ'_a(8)+δ_{oop}(CO)(8)+δ_{in}(C11C)(7)+Puck(7)+τ_a(7)+δ_{in}(C17C)(5)]+δ_{oop}(CH)(9)
482	482	531	2.3	9.13	R[τ'_a(45)+δ_{oop}(C17C)(22)+(δ_{in}(8)+δ_{oop}(5))(CO)]
468	468	498	2.2	4.58	δ_{oop}(NC5C)(40)+R[δ_{in}(CO)(11)+τ'_a(9)+δ'_a(6)]
448	448	476	0.9	7.24	(ρ'(49)+δ_{oop}(18))(NC5C)
438	439	473	1.8	2.92	R[δ_{in}(CO)(11)+Puck(7)+δ_{oop}(CO)(7)+δ_{oop}(C17C)(6)]+δ_{oop}(CH)(10)+(δ_{oop}(17)+ρ(5))(NC5C)
418	418	425	4.2	22.24	R[τ'_a(18)+δ_{in}(C17C)(7)+δ(CHO)(5)]+τ(CO3)(16)+δ_{sc}'($C17H_2$)(15)
401	402	418	1.3	3.35	δ_{oop}(NC5C)(26)+R[δ_a(14)+δ_{in}(CO)(6)+δ_{in}(C11C)(5)]+δ_{oop}(CH)(8)
366	367	392	2.5	3.40	δ_{oop}(NC5C)(34)+R[δ_{oop}(C11C)(6)+δ_a(6)]+δ_{oop}(CH)(6)
352	353	377	0.6	0.30	(δ_{oop}(50)+ρ'(26))(NC5C)
346	347	342	0.7	30.82	R[δ_{in}(C17C)](40)+δ_{sc}'($C17H_2$)(14)+τ(CO3)(9)+δ_{oop}(CH)(7)
337	338	332	7.7	46.07	(τ(49)+υ(5))(CO3)+δ_{sc}'($C17H_2$)(12)+R[τ(CO)](6)
308	309	314	1.1	11.43	(ρ(21)+δ_{oop}(11))(NC5C)+δ_{oop}(CH)(21) +R[τ_a](6)+υ(C6N)(5)
289	291	313	0.3	4.63	τ(C8C)(53)+R[τ_a(5)+δ_{oop}(C17C)(5)]+τ(C10C)(6)
288	289	297	1.4	7.91	R[δ_{oop}(C17C)(10)+τ_a(10)+δ_{oop}(C11C)(6)+δ_{in}(C17C)(5)]+τ(C8C)(11)+τ(C10C)(6)+δ_{oop}(CH)(6)+δ_{sc}'($C6H_2$)(5)
261	262	291	0.1	0.76	τ(C10C)(57)+τ(C9C)(28)
251	253	278	1.6	14.54	τ(C7C6)(16)+τ(C9C)(15)+τ(C10C)(13)+τ(CO1)(12)+τ(C8C)(11)+τ(C5N)(8)
235	236	240	6.7	120.90	τ(CO1)(71)+τ(C9C)(8)
211	213	218	1.2	8.30	τ(C9C)(21)+δ_{oop}(CH)(10)+τ(C7C6)(10)+δ_{sc}(NH)(8)+R[τ_a](5)
187	188	197	3.7	7.86	R[(τ(36)+δ_{oop}(16)+δ_{in}(9)(C17C))+τ_a(7)+δ_{oop}(C11C)(5)+τ'_a(5)]
173	174	187	0.8	4.31	R[δ_{in}(C11C)(33)+δ_{in}(C17C)(12)]+τ(C7C6)(10)+δ_{sc}'($C6H_2$)(8)
147	148	169	0.3	1.77	R[δ_{in}(C11C)(12)+τ_a(7)]+τ(C5N)(18)+τ(C9C)(15)+δ_{oop}(CH)(11)+τ(C7C6)(6)+τ(C10C)(5)
121	121	118	0.9	0.78	R[(τ(19)+δ_{in}(7))(C17C)+τ(CO)(19)+τ_a(12)+δ_{oop}(C11C)(5)]+δ_{oop}(CH)(13)+δ_{sc}'($C6H_2$)(5)+τ(C7C6)(5)
110	111	112	0.2	3.03	τ(C7C6)(21)+R[τ(C17C)(10)+τ(CO)(7)]+δ_{sc}'($C6H_2$)(15)+τ(C11C7)(7)+δ_{sc}(N)(6)
83	84	68	0.5	1.81	R[(τ (57)+δ_{in}(9))(C17C)+τ(CO)(14)]

53	54	52	1.5	1.97	τ(C11C7)(22)+τ(C6N)(21)+τ(C7C6)(14)+R[τ(CO)(6)+τ_a(5)]+δ(NH)(6)+τ(C5N)(6)
36	36	38	1.5	0.97	τ(C5N)(49)+τ(C9C)(16)+τ(C7C6)(11)+τ(C11C7)(8)
19	18	17	2.1	1.30	τ(C11C7)(47)+τ(C6N)(27)+δ_{oop}(CH)(7)+τ(C5N)(6)

Types of Vibration: υ: stretching, δ: deformation (bending), δ_{in}: in-plane bending, δ_{oop}: out-of-plane bending, ρ: rocking, τ: torsion, γ: scissoring, δ_a: deformation (asymmetric).

Aromatic Ring Vibrations

Salbutamol contains a substituted benzene ring, which shows characteristic vibrational bands. The C-H stretching vibrations were observed in the high-frequency region between 3078 cm^{-1} and 3094 cm^{-1}. The C-C ring stretching vibrations were identified in the mid-IR region, with prominent bands at 1604 cm^{-1} and 1504 cm^{-1}, in good agreement with experimental FT-IR data [10].

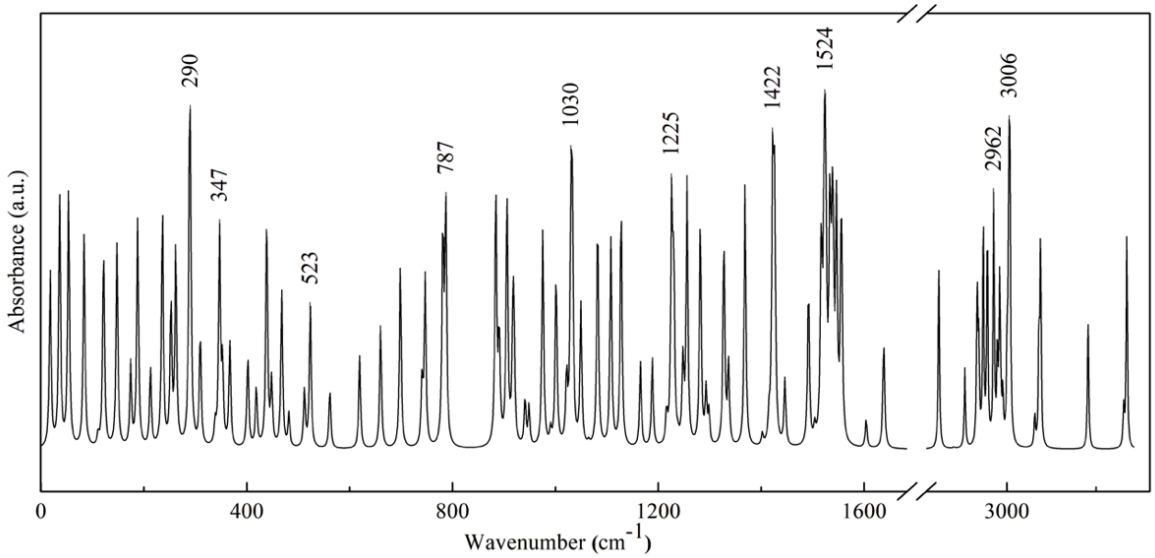

Fig. 3: FTIR Spectra of Salbutamol between 0-3400 cm^{-1} ranges at B3LYP/3-21G level.

Hydroxyl (-OH) Group Vibrations

The computed O-H stretching vibrations at 3336 cm^{-1} and 3327 cm^{-1} are in good agreement with the experimental FT-IR data reported by Ali et al. [10], who observed broad bands in the 3200-3600 cm^{-1} region indicative of hydrogen-bonded hydroxyl groups. The N-H stretch calculated at 3227 cm^{-1} also falls within the typical range for secondary amines and aligns with previous computational studies [12].

Methyl (-CH_3) Group Vibrations

The asymmetric and symmetric C-H stretching vibrations of the methyl groups were observed in the regions 2973-3008 cm^{-1} and 2916-2933 cm^{-1}, respectively. The corresponding deformation modes were found between 1523-1556 cm^{-1} (asymmetric) and 1422-1446 cm^{-1} (symmetric). These values are consistent with reported vibrations for aliphatic systems [17].

The low-frequency region (<500 cm^{-1}) is dominated by torsional motions and out-of-plane deformations, reflecting the molecular flexibility of the aliphatic side chain and ring substituents.

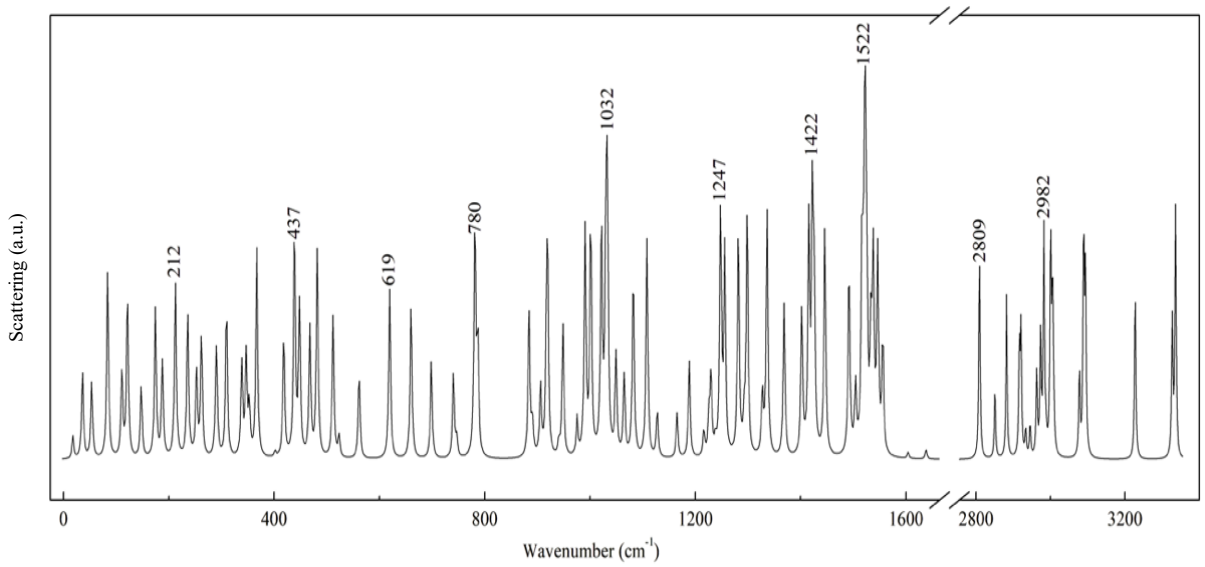

Fig. 4: Raman spectra plot of Salbutamol between the ranges 0-3400 cm^{-1} at B3LYP/3-21 G.

3.4 UV-Vis Spectral Analysis

From the table, it is clear that the main dipole transition occurs at 256 nm (H→L) with oscillator strength 0.040 and vertical excitation energy of 4.8 eV in the gas phase, whereas those values in water were 254 nm (H→L) with oscillator strength 0.044 and vertical excitation energy of 4.9 eV, and those values in ethanol occur at 254 nm (H→L) with oscillator strength 0.046 and vertical excitation energy of 4.9 eV as listed in Table 4.

Table 4: Calculated electronic properties (energy gap, absorption wavelengths, oscillatory strength and Dipole moments) of Salbutamol.

Phase	Transition states	Wavelength(nm)	Energy (eV)	Oscillator strength	Type of transition	Dipole moment
Gas	H→L	256	4.8	0.040	$\pi \rightarrow \pi^*$	3.882
	H-1→L	228	5.4	0.015		
	H→L+1	223	5.6	0.038		
Water	H→L	254	4.9	0.044		4.231
	H-1→L	240	5.2	0.003		
	H→L+1	225	5.5	0.074		
Ethanol	H→L	254	4.9	0.046		4.176
	H-1→L	239	5.2	0.025		
	H→L+1	224	5.5	0.081		

The HOMO-LUMO plots corresponding to H→L in gaseous, water, and ethanol phases are represented in Fig. 5. The energy difference ($\Delta E_g = E_{LUMO} - E_{HOMO}$) between the two molecular orbitals was 5.53 eV, 5.59 eV, and 5.59 eV, respectively, in the gas, water, and ethanol phases. The main electronic transition in the title molecule was found to be form π→ π*. The optimized (gas-phase) Salbutamol molecule has a computed dipole moment of 3.2035 D, indicating moderate molecular polarity. In contrast, the dipole moments calculated in solvent are larger (Table 4 shows 3.882 D in gas, 4.231 D in water, and 4.176 D in ethanol). This increase in the dipole moment in water and ethanol reflects enhanced polarization of the molecule in a polar environment - the solvent stabilizes charge separation, increasing the overall dipole moment in solution suggests stronger interactions with polar media or receptors. The difference between the optimized-structure value (3.2035 D) and the gas-phase value (3.8816 D) arises from calculation conditions and demonstrates consistency in the trend of polarity. polarity of Salbutamol. In practical terms, a higher The UV absorption plot of Salbutamol in the gas phase shows one distinct peak, indicating specific electronic transitions within the molecule.

The most significant peak at 191 nm, represents the primary electronic transition with the highest probability and energy absorption. The UV absorption plot of Salbutamol in a water solvent displays one key absorption peak at 190.4 nm, indicating electronic transitions within the Salbutamol molecule. The UV plot of Salbutamol in ethanol also shows one distinct absorbance peak. The most prominent peak is at 191 nm.

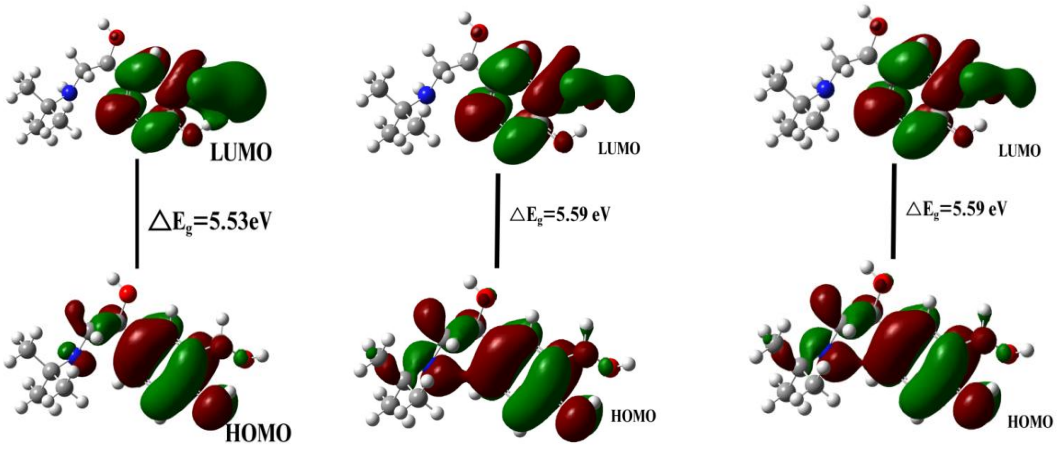

Fig. 5: HOMO-LUMO plot of Salbutamol in gas, water and ethanol respectively.

3.5 Molecular Electrostatic potential (MEP) Surface

The Molecular Electrostatic Potential (MEP) provides a visual representation of the charge distribution within a molecule, which is essential for understanding electrophilic and nucleophilic reactivity. Mathematically, the MEP at a point r in the space around a molecule (in atomic units) can be expressed as [26]:

$$V(r) = \sum_A \frac{z_A}{|\vec{R}_A - \vec{r}|} - \int \frac{\rho(\vec{r_1}')dr'}{|r' - r|}$$

In the present study, the MEP surface of Salbutamol was generated using the optimized geometry obtained at the DFT/B3LYP level with the 3-21 basis set. The MEP is color-mapped onto the molecular van der Waals surface, where red indicates regions of most negative electrostatic potential (attractive to electrophiles), and blue represents most positive potential (attractive to nucleophiles), with green showing regions of neutral potential. The visualized MEP surface of Salbutamol (Fig. 6 left) shows that, red regions are concentrated around the hydroxyl (-OH) groups and oxygen atoms, indicating electron rich sites that are prone to electrophilic attack. Blue regions are primarily located near hydrogen atoms attached to the aromatic ring and amine group, suggesting electron deficient sites favorable for nucleophilic interactions. Green zones, representing areas of zero potential, are generally seen over the non-polar regions such as methyl groups and hydrocarbon chains. The contour plot in Fig. 6(right) offers a detailed two-dimensional perspective on the molecular electrostatic potential (MEP) distribution of Salbutamol. Contour lines, each representing a constant value of electrostatic potential, allow for precise identification of regions with similar electronic character across the molecular surface. Closely spaced contour lines indicate rapid changes in potential, often found adjacent to highly electronegative atoms such as oxygen, while wider spacing suggests more gradually varying regions, typical of non-polar groups like methyl or hydrocarbon chains.

3.6 ADMET Property Analysis

In this section, we present the ADMET (Absorption, Distribution, Metabolism, Excretion, and Toxicity) profile of Salbutamol, predicted using the SwissADME and pkCSM web tools. These in silico assessments are essential for early-stage evaluation of pharmacokinetic behavior and safety.

Salbutamol's drug-likeness was first evaluated against Lipinski's "Rule of Five", which stipulates that, for good oral bioavailability. As shown in Table 5, Salbutamol (MW = 239.31 g/mol; H-bond donors = 4; acceptors = 4; rotatable bonds = 5; WLogP = 0.83) violates none of these criteria, confirming its compliance with Lipinski's guidelines. Salbutamol's LD_{50} was predicted as 2.395 mol/kg (~573 g/kg), placing it well above 5000 mg/kg; thus, it falls into Class VI (non-toxic) upon oral administration [27]. Passive gastrointestinal absorption (HIA) and blood-brain barrier (BBB) permeation were assessed using the BOILED-Egg model on SwissADME. Salbutamol (TPSA = 72.72 Å²; WLogP = 0.83) lies squarely within the white region (high HIA) but outside the yolk (limited BBB permeation), and is colored red (non-P-gp substrate), indicating favorable oral absorption and negligible brain entry (Fig. 7).

The bioavailability radar further highlights Salbutamol's pharmacokinetic fitness by overlaying six physicochemical descriptors (lipophilicity, size, polarity, solubility, flexibility, saturation) against optimal ranges. All parameters fall within the "pink" optimal polygon, and its bioavailability score of 0.55 confirms good overall oral bioavailability.

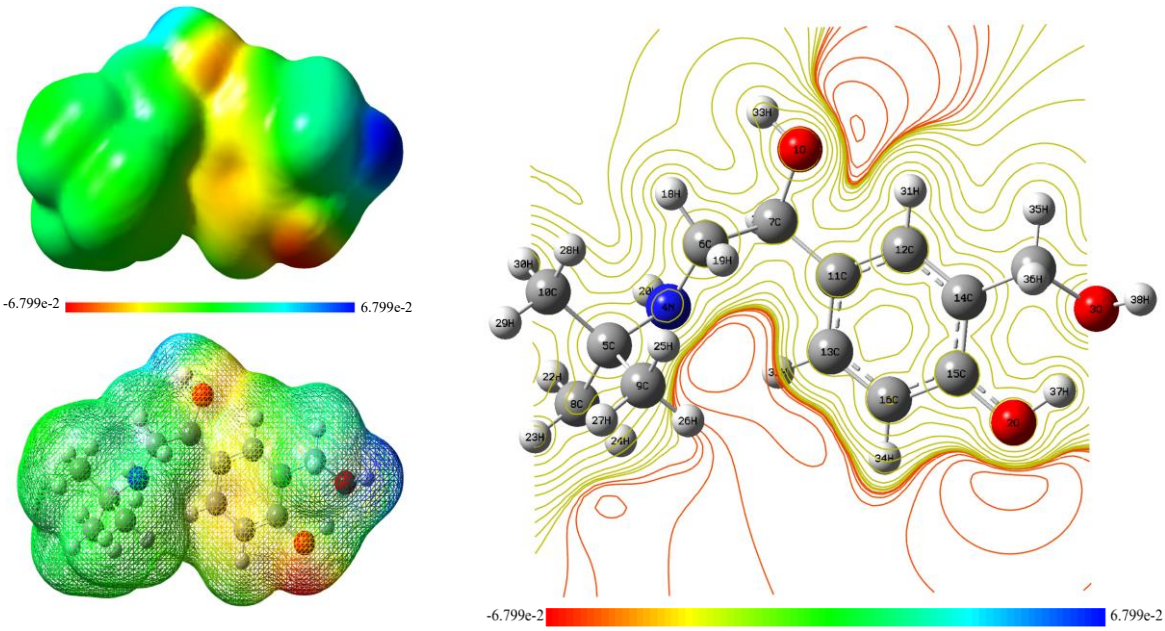

Fig. 6: (a) Molecular electrostatic potential map, and (b) Contour plot of molecular electrostatic potential surface of Salbutamol.

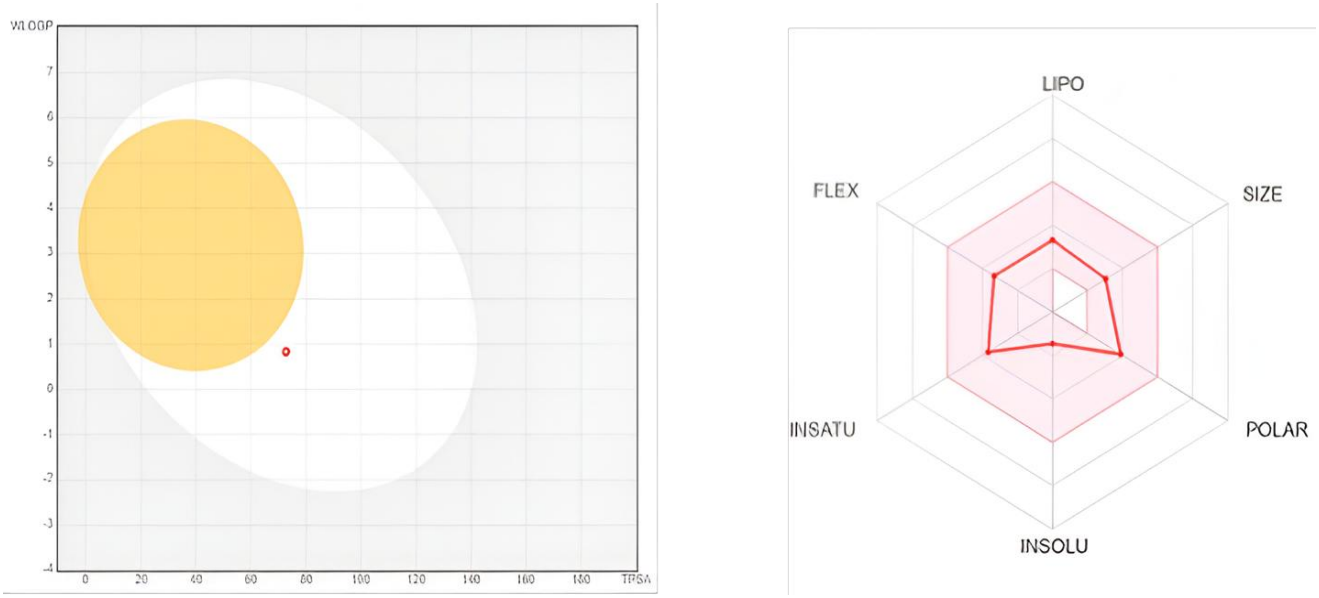

Fig. 7: Swiss ADME boiled egg model and bioavailability radar chart for Salbutamol.

Table 5: The different ADMET parameters for Salbutamol.

Parameters	Value	Parameters	Value
Molecular weight(g/mol)	239.31	Lipophilicity (WlogP)	0.83
Rotatable bond	5	Water solubility (logS)	-1.45
Hydrogen bond acceptor	4	Permeability coefficients (log Kp cm/s)	-7.54
Hydrogen bond donor	4	Lipinski violations	0
Topological polar surface area ($Å^2$)	72.72	GI absorption	High
Molar refractivity	67.60	Synthetic accessibility	2.30

Blood brain-barrier permeate	No	Bioavailability score	0.55
P-glycoprotein substrate	No	Lethal Dose (LD 50)	2.395l/kg

3.7 Molecular Docking

Molecular docking studies were performed to predict the binding mode and affinity of Salbutamol with the human β_2-adrenergic receptor (PDB ID: 3NY8). Blind docking using SwissDock generated 20 potential binding modes. The top-ranked pose, with a calculated binding affinity of -7.545 kcal/mol, indicated the most favorable interaction. The full list of binding affinities for all clusters is provided in Table 6.

Table 6: Calculated Binding Affinities (kcal/mol) of Salbutamol β_2 Adrenergic Receptor Complex Obtained from SwissDock.

Model	Calculated affinity (kcal/mol)	Model	Calculated affinity (kcal/mol)	Model	Calculated affinity (kcal/mol)
1	-7.545	8	-6.519	15	-6.186
2	-7.058	9	-6.411	16	-6.137
3	-6.730	10	-6.407	17	-5.989
4	-6.599	11	-6.393	18	-5.862
5	-6.552	12	-6.310	19	-5.823
6	-6.541	13	-6.293	20	-5.729
7	-6.519	14	-6.223		

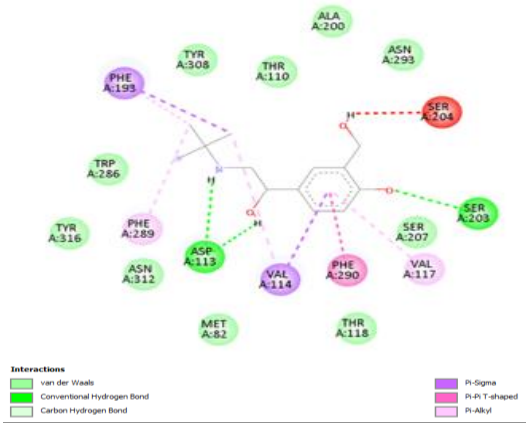

Fig. 8: 2D- ligand interaction diagram of Salbutamol with 3NY8.

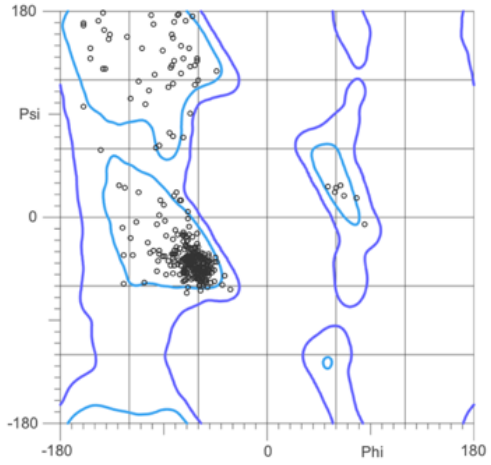

Fig. 9: Ramachandran plot of protein 3NY8.

The visualization of the ligand-receptor complex was performed using BIOVIA Discovery Studio Visualizer, which revealed significant hydrogen bonding and hydrophobic contacts within the binding cavity. The 2D interaction diagram (Fig. 8) shows that Salbutamol forms multiple hydrogen bonds with key residues in the receptor, which are crucial for stability and activity. The 3D docked structures (Fig. 10) illustrate how Salbutamol is situated within the hydrophobic pocket of the protein, aligned along the active site groove and stabilized by non-covalent interactions.

To assess the conformational quality of the protein structure, a Ramachandran plot was generated using MolProbity, which demonstrated that most residues lie within the allowed and favored regions, suggesting the receptor is sterically stable and suitable for docking. The plot is shown in Fig. 9.

The observed binding mode is consistent with the electronic properties revealed by the MEP and Mulliken charge analyses. The hydrogen bond formation with ASP113 and ASN312 involves the positively charged hydrogen atoms of the protonated amine and hydroxyl groups, which were identified as strong hydrogen bond donors (high positive Mulliken charges on H20, H37, H38). Furthermore, the electron-

rich oxygen atoms (O1, O2, O3), which showed highly negative MEP regions, are positioned to act as hydrogen bond acceptors with surrounding water molecules or protein residues not visible in the docking pose.

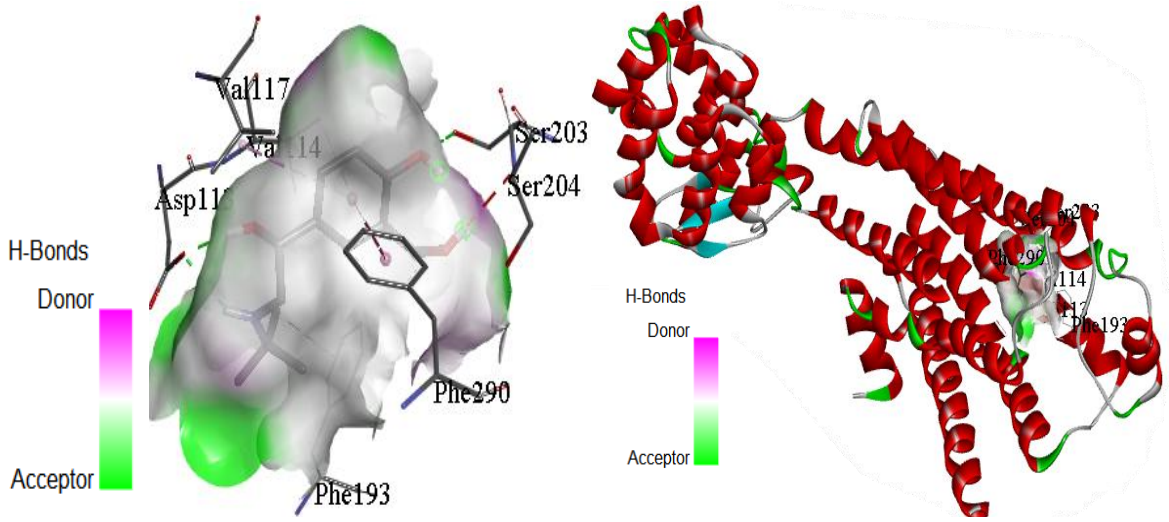

Fig. 10: Docked 3D structure showing binding pocket and with receptor binding pocket in terms of H-bond.

4. CONCLUSION

This study provides a comprehensive computational profile of Salbutamol by integrating DFT and molecular docking analyses. The optimized molecular geometry confirms the expected structural features, while the vibrational assignments, including key O-H, N-H, and C-H stretches, are consistent with literature and confirm the reliability of the computational model. Electronic property analysis revealed a HOMO-LUMO gap of 5.53 eV, indicating moderate chemical stability, and a significant increase in dipole moment in polar solvents, highlighting its solvation behavior. Crucially, molecular docking with the β_2-adrenergic receptor (3NY8) yielded a strong binding affinity (-7.545 kcal/mol), rationalizing its pharmacological activity. The binding pose shows critical interactions: hydrogen bonds with ASP113 and ASN312, and hydrophobic contacts with VAL114, VAL117, and PHE290. A clear structure-activity relationship for salbutamol is established by integrating these data from molecular structure and electronic distribution to receptor binding. This provides important insights for the logical design of new and more potent β_2-agonist medications.

AUTHOR CONTRIBUTION

D. Joshi: Writing-original draft, Investigation, and Formal analysis; B.D. Joshi: Methodology, Writing-review and Editing, Conceptualization, and Supervision.

CONFLICTS OF INTEREST

There are no conflicts to declare.

ACKNOWLEDGEMENTS

Authors acknowledge to Siddhanath Science Campus for providing lab facility and Prof. Poonam Tandon, Deen Dayal Gorakhpur University, Gorakhpur, India for providing Gaussian software.

REFERENCES

[1] L. Marques, N. Vale, Salbutamol in the management of asthma: A review, *International Journal of Molecular Sciences*, **23** (2022) 14207. https://doi.org/10.3390/ijms232214207

[2] J.P. Beale, N.C. Stephenson, A structural study of a pyridine inclusion compound of bis (dimethyl-o-thiolophenylarsine) palladium (II), *Structural Science*, **28** (1972) 557-60. https://doi.org/10.1107/S0567740872002742

[3] I.P. Hall, Bronchohdilators, Beta Agonists, Encyclopedia of Respiratory Medicine, Academic Press, (2022), 288-292, ISBN 9780123708793

[4] L.E. Martin, J.C. Hobson, J.A. Page, C. Harrison, Metabolic studies of salbutamol-3H: A new bronchodilator, in rat, rabbit, dog and man. *European Journal of Pharmacology*, **14** (1971) 183-99, 183-199. https://doi.org/10.1016/0014-2999(71)90211-1

[5] A.E. Tribe, R.M. Wong, J.S. Robinson, A controlled trial of intravenous salbutamol and aminophylline in acute asthma, *Medical Journal of Australia*, **2** (1976) 749-52. https://doi.org/10.5694/j.1326-5377.1976.tb128275.x

[6] W. MacNee, N.J. Douglas, M.F. Sudlow, Effects of inhalation of beta-sympathomimetic and atropine-like drugs on airway calibre in normal subjects, *Clinical Science*, **63** (1982) 137-43. https://doi.org/10.1042/cs0630137

[7] F. Riedel, H. von der Hart, Variable response to inhaled salbutamol of different lung function parameters in healthy children, *Lung*, **164** (1986) 333-8. https://doi.org/10.1007/BF02713658

[8] C.A. Sorbini, V. Grassi, C. Tantucci, L. Corea, M. Bentivoglio, P. Verdecchia, M. Motolese, Ventilatory effects of selective beta 1-(prenalterol) or beta 2-(salbutamol) adrenoceptor agonism in man, *International Journal of Clinical Pharmacology, Therapy, and Toxicology*, **22** (1984) 570-5 .https://pubmed.ncbi.nlm.nih.gov/6150902

[9] H. Allen, S.H. Backhouse, J.H. Hull, O.J. Price, Anti-Doping policy, therapeutic use exemption and medication use in athletes with asthma: a narrative review and critical appraisal of current regulations, Sports *Medicine*, **49** (2019) 659-68. https://doi.org/10.1007/s40279-019-01075-z

[10] H.R. Ali, H.G. Edwards, J. Kendrick, I.J. Scowen, Vibrational spectroscopic study of salbutamol hemisulphate, *Drug testing and analysis*, **1**(2009) 51-6. https://doi.org/10.1002/dta.8

[11] S. Bandaru, G. Tiwari, J. Akka, V. Kumar Marri, M. Alvala, Ravi V. Gutlapalli, A. Nayarisseri, H. Prasad Mundluru, Identification of high affinity bioactive Salbutamol conformer directed against mutated (Thr164Ile) beta 2 adrenergic receptor, *Current topics in medicinal chemistry,* **15** (2015) 50-6. https://doi.org/10.2174/1568026615666150112113040

[12] R. Omer, P. Koparır, L. Ahmed, M. Koparır, Computational determination the reactivity of salbutamol and propranolol drugs, *Turkish Computational and Theoretical Chemistry,* **4** (2020) 67-75. https://doi.org/10.33435/tcandtc.768758

[13] A.J. Al-Ani, P.M. Szell, Z. Rehman, H. Blade, H.P. Wheatcroft, L.P. Hughes, S.P. Brown, C.C. Wilson, Combining X-ray and NMR Crystallography to Explore the Crystallographic Disorder in Salbutamol Oxalate, *Crystal Growth & Design*, **22** (2022) 4696-707. https://doi.org/10.1021/acs.cgd.1c01093

[14] T. Zhao, Z. Liu, J. Niu, B. Lv, Y. Xiao, Y. Li, Investigation of the interaction mechanism between salbutamol a human serum albumin by multispectroscopic and molecular docking, *BioMed Research International*, **1** (2020) 1693602. https://doi.org/10.1155/2020/1693602

[15] H.E. Pence, A. Williams, ChemSpider: an online chemical information resource, Journal of Chemical Education, 87(2010) 1123-1124. https://doi.org/10.1021/ed100697w

[16] C. Lee, W. Yang, R.G. Parr, Development of the Colle-Salvetti correlation-energy formula into a functional of the electron density, *Physical Review B*, **37** (1988) 785. https://doi.org/10.1103/PhysRevB.37.785R

[17] B.D. Joshi, J.B. Khadka, A. Bhatt, Structure, electronic and vibrational study of 7-methyl-2, 3-dihydro-(1, 3) thiazolo (3, 2-a) pyrimidin-5-one by using density functional theory. *Journal of Institute of Science and Technology*, 22(2018) 1-11. https://doi.org/10.3126/jist.v22i2.19589\

[18] P. Pulay, G. Fogarasi, F. Pang, J.E. Boggs, Systematic ab initio gradient calculation of molecular geometries, force constants, and dipole moment derivatives, *Journal of the American Chemical Society*, **101** (1979) 2550-60. https://doi.org/10.1021/ja00504a009

[19] G. Fogarasi, X. Zhou, P.W. Taylor, P. Pulay, The calculation of ab initio molecular geometries: efficient optimization by natural internal coordinates and empirical correction by offset forces, *Journal of the American Chemical Society*, **114** (1992) 8191-201. https://doi.org/10.1021/ja00047a032

[20] A.J. Frisch, A.B. Nielson, A.J. Holder, GaussView user manual, Gaussian Inc., Pittsburgh, PA, (2000) 556.

[21] H. Yoshida, K. Takeda, J. Okamura, A. Ehara, H. Matsuura, A new approach to vibrational analysis of large molecules by density functional theory: wavenumber-linear scaling method, *The Journal of Physical Chemistry A*, **106** (2002) 3580-6. https://doi.org/10.1021/jp013084m

[22] M.E. Casida, K.C Casida, D.R. Salahub, Excited-state potential energy curves from time-dependent density-functional theory: A cross section of formaldehyde's 1A1 manifold, *International Journal of Quantum Chemistry*, **70** (1998) 933-41. https://doi.org/10.1002/(SICI)1097-461X(1998)70:4/5<933::AID-QUA39>3.0.CO;2-Z

[23] O. Trott, A.J. Olson, AutoDock Vina: improving the speed and accuracy of docking with a new scoring function, efficient optimization, and multithreading. *Journal of computational chemistry,* **31** (2010) 455-61. https://doi.org/10.1002/jcc.21334

[24] G.M. Morris, R. Huey, W. Lindstrom, M.F. Sanner, R.K. Belew, D.S. Goodsell, A.J. Olson, AutoDock4 and AutoDockTools4: Automated docking with selective receptor flexibility, Journal of computational chemistry, **30** (2009) 2785-91. https://doi.org/10.1002/jcc.21256

[25] M. Bugnon, U.F. Röhrig, M. Goullieux, M.A. Perez, A. Daina, O. Michielin, V. Zoete, SwissDock 2024: major enhancements for small-molecule docking with AttractingCavities and AutoDock Vina, *Nucleic acids research,* **52** (2024) 324-32. https://doi.org/10.1093/nar/gkae300

[26] R. Parthasarathi, V. Subramanian, P.K. Chattaraj, Effect of electric field on the global and local reactivity indices, *Chemical Physics Letters*, **382** (2003) 48-56. https://doi.org/10.1016/j.cplett.2003.09.160

[27] A. Daina, O. Michielin, V. Zoete, SwissADME: a free web tool to evaluate pharmacokinetics, drug-likeness and medicinal chemistry friendliness of small molecules, *Scientific Reports*, **7** (2017) 42717. https://doi.org/10.1038/srep42717